Host oligodendrogliopathy and α-synuclein strains dictate disease severity in multiple system atrophy

Torre-Muruzabal Teresa,[1] Van der Perren Anke,[1] Coens Audrey,[2] Gelders Géraldine,[1] Barber Janer Anna,[1] Camacho-Garcia Sara,[1] Klingstedt Therése,[4] Nilsson Peter,[4] Stefanova Nadia,[3] Melki Ronald,[2] Baekelandt Veerle[1] and Peelaerts Wouter[1]

1 KU Leuven, Laboratory for Neurobiology and Gene Therapy, Department of Neurosciences, Leuven, Belgium

2 Institut François Jacob (MIRCen), CEA, and Laboratory of Neurodegenerative Diseases, CNRS, Fontenay-aux-Roses, France

3 Division of Neurobiology, Department of Neurology, Medical University of Innsbruck, Innsbruck, Austria

4 Department of Physics, Chemistry and Biology, Linköping University, Linköping, Sweden

Correspondence to: Wouter Peelaerts

Laboratory for Neurobiology and Gene Therapy, ON 5b, Herestraat 49 – Box 1023, 3000 Leuven, Belgium

E-mail: wouter.peelaerts@kuleuven.be

Correspondence may also be addressed to: Veerle Baekelandt

E-mail: veerle.baekelandt@kuleuven.be

Running title: Host and αSyn strains interact in MSA

Abstract

Multiple system atrophy is a progressive neurodegenerative disease with prominent autonomic and motor features. During early stages different subtypes of multiple system atrophy are distinguished by their predominant parkinsonian or cerebellar symptoms reflecting the heterogeneous nature of the disease. The pathognomonic feature of multiple system atrophy is the presence of α-synuclein (αSyn) protein deposits in oligodendroglial cells. αSyn can assemble in specific cellular or disease environments and form αSyn strains with unique structural features but the ability of αSyn strains to propagate in oligodendrocytes remains elusive.

More recently, it was shown that multiple multiple system atrophy strains with related conformations exist in the brain of patients. Here, we investigated if different αSyn strains can influence multiple system atrophy progression in a strain-dependent manner. To this aim, we injected two recombinant αSyn strains (fibrils and ribbons) in multiple system atrophy transgenic mice and found that αSyn protein strains determine disease severity in multiple system atrophy via host-restricted and cell-specific pathology *in vivo*.

αSyn strains significantly impact disease progression in a strain-dependent way via oligodendroglial, neurotoxic and immune-related mechanisms. Neurodegeneration and brain atrophy were accompanied by unique microglial and astroglial responses and the recruitment of central and peripheral immune cells. The differential activation of microglial cells correlated with the structural features of αSyn strains both *in vitro* and *in vivo*. Spectral analysis showed that ribbons propagate oligodendroglial inclusions that are structurally distinct from those of fibrils, with resemblance to oligodendroglial inclusions in multiple system atrophy patient brain.

This study therefore shows that the multiple system atrophy phenotype is governed by both the αSyn strain nature and the host environment and that by injecting αSyn strains in a multiple system atrophy animal model a more comprehensive phenotype can be established.

Keywords: multiple system atrophy; neurodegeneration; α-synuclein strains; synucleinopathy

Abbreviations: AAV = adeno associated viral vector; αSyn = α-synuclein; BSA = bovine serum albumin; CD = cluster of differentiation; DARPP = dopamine- and cAMP-regulated phosphoprotein; DIV = days in vitro; DMEM = Dulbecco's Modified Eagle Medium; EM = electron microscopy; EU = endotoxin units;

GCIs = glial cytoplasmic inclusions; GFAP = glial fibrillary acidic protein; h-FTAA = hepta-formylthiophene acetic acid; HLA = human leukocyte antigen; IL = interleukin; LCO = luminescent conjugated oligothiophenes; PLP = proteolipid protein; PMCA = protein misfolding cycling amplification assay; MSA = multiple system atrophy; MHC = major histocompatibility complex; OPCA = olivopontocerebellar atrophy; SND = striatonigral degeneration; SNpc = substantia nigra pars compacta;TH = tyrosine hydroxylase; TLR = toll-like receptor; TNFα = tumor necrosis factor α; TMEM = transmembrane; WT= wild type

Introduction

Multiple system atrophy is a rare neurodegenerative syndrome of unknown etiology. It comprises a group of neurological syndromes, including the Shy-Drager syndrome, olivopontocerebellar atrophy (OPCA) and striatonigral degeneration (SND). Today, OPCA and SND are classified as multiple system atrophy with predominant cerebellar ataxia or parkinsonism.[1] Several years before the appearance of motor symptoms, autonomic features such as urogenital dysfunction or orthostatic hypotension develop during a protracted and prodromal phase.[1–4] These autonomic features are highly variable between patients and underscore the heterogeneity of the disease.

Central to MSA pathology is the accumulation of α-synuclein (αSyn) protein in oligodendrocytes.[5] αSyn is invariably found in insoluble deposits in oligodendrocytes of postmortem multiple system atrophy brain and identification of glial cytoplasmic inclusions (GCIs) is required for a definite diagnosis of multiple system atrophy. αSyn-rich inclusions are also found in the brain of people with other synucleinopathies, such as Parkinson's disease and dementia with Lewy bodies, but the conformational properties of αSyn aggregates were shown to be specific for multiple system atrophy.[6] The structure of MSA fibrils purified from human brain analyzed by cryo-EM was found to be highly organized into β-sheet rich filaments that bundle into a twisted fibrillar scaffold[7]. We and others showed that αSyn assemblies isolated, purified and amplified from multiple system atrophy brain have different biological activities compared to those isolated from the brain of people with Parkinson's disease or dementia with Lewy bodies[8–11]. This indicates that a structure-function relationship exists within αSyn strains and that they might influence disease phenotypes in different synucleinopathies.

Because of their unique structural characteristics in different synucleinopathies, αSyn aggregates behave as prion strains. Multiple system atrophy strains are highly neurotoxic and amplify *in vivo* via seeded templating of soluble αSyn in oligodendrocytes. Even though it has been shown that MSA strains can efficiently propagate in a permissive environment, it is not known if multiple system atrophy strains characteristics are maintained within different cellular or disease environments where host restriction might affect strain properties. In the case of human prion diseases, prion strains are not monoclonal.[7,12] Instead, they comprise a cloud of assemblies often with a dominant strain that is maintained and propagated under host selection.[13] The conformation of αSyn within fibrillar aggregates purified from multiple system atrophy patients brain homogenates displays subtle differences. The relative abundance of the different polymorphs also varies in different tissues (e.g. the cerebellum and putamen). This

suggests that an ensemble of multiple system atrophy strains might also exist in multiple system atrophy brains.[7]

The diversity of αSyn strains in synucleinopathies raises the question if different strains might influence oligodendroglial and neuropathology or inflammatory processes, which are central to multiple system atrophy,[14] but this has never been experimentally tested. We therefore asked if αSyn strains can determine MSA disease outcome. To that aim, we injected two well-characterized but structurally distinct recombinant αSyn strains (fibrils and ribbons) in transgenic multiple system atrophy mice that constitutively express αSyn in oligodendrocytes.[15] We found that in an multiple system atrophy disease environment the two strains dictate distinct disease phenotypes. Fibrils caused an aggressive and toxic phenotype with severe myelin loss and neurodegeneration. Ribbons, however, caused a milder neurotoxic phenotype but a distinct type of glial pathology reflected by conformationally distinct oligodendroglial inclusions that resemble those of multiple system atrophy. In addition, αSyn fibrils caused a significant pro-inflammatory response and microglial activation with recruitment of peripheral myeloid and leukocytic cells. Because of unique seeding capacities in the oligodendroglial milieu and the pro-inflammatory features of αSyn strains, the introduction of fibrillar seeds into the multiple system atrophy model resulted in a disease phenotype that mimics to a higher extent the clinical condition.

Materials and Methods

Generation and labelling of αSyn assemblies

αSyn fibrils and ribbons were generated and characterized by transmission electron microscopy and by limited proteolysis profiling as previously described in detail.[16] The nature of the αSyn assemblies used was routinely assessed using a Jeol 1400 (Jeol Ltd, Peabody, MA) Transmission Electron Microscope after adsorption of the samples onto carbon-coated 200-mesh grids and negative staining with 1% uranyl acetate. The images were acquired with a Gatan Orius CCD camera (Gatan). The endotoxin levels were quantified in all αSyn preparations as described previously.[17] The endotoxin levels were below 0.02 endotoxin units/mg (EU/mg) based on the use of the Pierce LAL Chromogenic Endotoxin Quantification Kit.

Isolation of primary microglia

Primary microglia were derived from P0-P1 C57BL/6 mouse brain. Briefly, after removal of the meninges, the brains were placed in tubes containing Hanks' Balanced Salt solution (Sigma-Aldrich). Next, they were incubated with 1% trypsin (Gibco-BRL, Life Technologies) for 10 min at 37°C. Following a mechanical dissociation in DMEM supplemented with DNaseI (Sigma-Aldrich), cells were collected by centrifugation for 10 min at 1200 rpm and re-suspended in DMEM, 10% heat-inactivated FCS and 1% Penicillin-Streptomicin and plated in a 75 cm^2 culture flask. On days 10-14, to collect microglial cells, the microglia–astrocyte co-cultures were shaken on a rotary shaker at 400 rpm for 3 hours. Microglial cells were plated at a density of 300 000 cells/well in a 12-well plate with coverslips. At DIV 14 cells were treated with the different αSyn assemblies.

Recombinant αSyn administration and q-PCR

Cells were treated with the different αSyn assemblies at a concentration of 1 µM. Untreated cells and cells incubated with BSA as control. After 24 hours the total RNA was extracted from each well and 1 µg of total RNA of primary microglial cells were reverse-transcribed using the High-Capacity cDNA Archive kit (Applied Biosystems, Carlsbad, USA), according to manufacturer's instructions. cDNA was used in triplicates as template for q-PCR amplification with specific primers and probes for each microglial marker as described in **Supplementary table 1**. Cycling conditions were 10 minutes at 95°C, followed by 50 cycles of 10 seconds at 95°C and 30 seconds at 55°C. The obtained mRNA levels were normalized to the mRNA levels of HPRT housekeeping gene.

Animals and stereotactic injection

All animal experiments were carried out in accordance with the European Communities Council Directive of November 24, 1986 (86/609/EEC) and approved by the Bioethical Committee of the KU Leuven (Belgium). Approximately 5 month old male and female transgenic (PLP-hαSyn mice[15]) housed under a normal 12-hour light/dark cycle with free access to pelleted food and tap water. All surgical procedures were performed using aseptic techniques and ketamine (70 mg/kg intraperitoneal [i.p.], Ketalar, Pfizer, Belgium) and medetomidine (1 mg/kg, Dormitor, Pfizer) anesthesia. Following anesthesia, the rodents were placed in a stereotactic head frame (Stoelting, IL, USA), a midline incision of the skin was made, and a small hole drilled in the skull at the appropriate location, using bregma as

reference. Injections were performed with a 30-gauge needle and a 10µL Hamilton syringe. Animals were injected with 2µL containing 5µg of recombinant protein (BSA, fibrils or ribbons). Stereotactic coordinates used for the dorsal striatum were anteroposterior, +0.5; lateral, -2.0; and dorsoventral, -3.3 calculated from the dura using bregma as reference. The injection rate was 0.25 µL/min and the needle was left in place for an additional 5 minutes before being retracted. Animals were sacrificed after behavioral analysis 9 months post-stereotactic injection (number of animals injected with BSA = 9, fibrils = 12 and ribbons = 7).

Behavioral tests

To examine side bias in spontaneous forelimb use, mice were placed individually inside a glass cylinder (12 cm diameter, 22 cm height). A total of 30 contacts (with fully extended digits executed with both forelimbs) were recorded for each animal. Video-recordings were examined by an observer blinded to the animal's identity to count the number of touches. The number of impaired forelimb contacts was expressed as a percentage of total forelimb contacts. Non-lesioned control mice should score around 50% in this test. For the pole test, a wooden vertical pole with rope, 1.5 cm of diameter and 50 cm high was used and placed in an open cage. Each mouse was placed with the head up at the top of the pole and the time for turning downwards (T-turn) as well as the total time for climbing down the pole until the mouse reached the floor with the four paws (T-total) was taken in 5 trials. We performed the test 3 times per test and the average of the 3 trials was used for statistical analysis.

Immunocytochemistry

Cells were washed in PBS followed by a permeabilization step in a 0.1% Triton-X100 in PBS solution for 5 min. Next a blocking step of 20 minutes with 10% goat serum in PBS was performed. Cells were incubated with rat anti human αSyn 15G7 primary antibodies (Enzo Life Sciences, 1:500) and rabbit anti-Iba1 (Wako, 1:500) overnight at room temperature. The next day, after 3 washes with PBS cells were incubated with secondary antibody (Alexa Fluor conjugated antibody, 1:500, Molecular probes, Invitrogen) for 1 hour at room temperature. After being rinsed in PBS, coverslips were closed with Mowiol (Calbiochem®, California, US) and DAPI (1:1000). Fluorescent stainings were visualized by confocal microscopy with an LSM 510 unit (Zeiss, Belgium) or a Nikon-Märzhäuser Slide Express 2 microscope in combination with a Plan Apo 10x objective (NA 0.45) was used. The setup was controlled by NIS-Elements (5.21.03, Nikon Instruments Europe B.V.) .

MSA patients

Paraffin-embedded human brain tissue from MSA subjects and age-matched control subjects were obtained from the Institute Born-Bunge (IBB) NeuroBioBank (BB190113), Antwerp, Belgium (**Table 1**). All MSA cases were examined and confirmed for oligodendroglial αSyn pathology. Protocols were reviewed and approved by the Antwerp University and KU Leuven University Institutional Review boards.

Immunohistochemistry

Mice were anesthetized by intraperitoneal injection of pentobarbital (60 mg/kg, Nembutal, Ceva Sante Animale) and perfused transcardially with saline followed by ice-cold 4 % paraformaldehyde (PFA) in phosphate buffered saline (PBS). Isolation and perfusion were followed by overnight fixation in 4 % PFA. For DAB staining, free-floating sections were pretreated with 3 % hydrogen peroxide (Chem-Lab) in PBS and 10% Methanol for 10 min and incubated overnight with the primary antibody (**Supplementary table 2**) in PBS/T 0.1 with 10 % normal swine/ goat or rabbit serum (Dako). Second, a biotinylated swine anti-rabbit, goat or rabbit (1:300, Dako) was used, followed by incubation with a streptavidin–HRP complex (1:1000, Dako). Immunoreactivity was visualized using DAB (0.4 mg/ml, Sigma-Aldrich) or Vector SG (Vector Laboratories) as a chromogen. After a dehydration series, stained sections were mounted with DPX (Sigma-Aldrich) and visualized with a light microscope (Leica Microsystems).

For fluorescent double or triple staining, sections were washed in PBS, pre-blocked with 10 % normal horse serum in PBS/T 1 % and incubated overnight with the primary antibodies in PBS/T 1 % with 10 % donkey serum. After washing with PBS, sections were incubated for 2 h with donkey secondary antibodies with different fluorescent tags (1:500, PBS/T 1 %). When staining with the luminescent conjugated oligothiophene (LCO) h-FTAA, an additional staining step after secondary antibody labeling was performed. The synthesis of h-FTAA has been published elsewhere.[18] Slides were incubated with 1µM of h-FTAA for 45 minutes in PBS after which they are washed with PBS two times and one additional time with 10% Mowiol in PBS for 10 minutes. Tissue slides were mounted with Mowiol. For myelin detection, Fluoromyelin (ThermoFisher, F34651) was used. Sections were incubated in a concentration of fluoromyelin of 1:300 in PBS Triton (1%) for 30 minutes in the dark and washed in PBS. Fluorescence was detected either with Leica DM6 B automated upright microscope and images were taken using the Leica DFC7000 T camera. Spectral analysis of h-FTAA was done by confocal microscopy

with a Zeiss LSM 880 – Airyscan. (Cell and Tissue Imaging Cluster (CIC), Supported by Hercules AKUL/15/37_GOH1816N and FWO G.0929.15 to Pieter Vanden Berghe, KU Leuven).

Human paraffin brain tissue was sectioned at 6 µm. Slides were heated at 75˚C in an oven for 20 min and rehydrated via serial rehydration in xylene, 100% ethanol, 90% ethanol and 70% ethanol and distilled water. Antigen retrieval was performed with the universal HIER antigen retrieval reagent (Abcam) for 30 minutes in a steam cooker at 95-100˚C. For immunofluorescent analysis, sections were blocked with 10% donkey serum (Millipore-Sigma) in 0.1% Triton-X in PBS for 30 min at room temperature. For antigen detection, different concentrations of primary antibodies are listed in **Supplementary table 2** and were used at 4˚C overnight. Sections were triple washed in 0.1% Triton-X in PBS and incubated with secondary antibody (**Supplementary table 2**) and 1:1000 DAPI for two hours at room temperature after which the sections were washed again with 0.1% Triton-X in PBS. Slides were incubated with 1µM of h-FTAA for 30 minutes in PBS after which they are washed with PBS two times and one additional time with 10% Mowiol in PBS for 10 minutes. After drying, slides were treated with Trueblack Lipofuscin Autofluorescent Quencher (Biotium) for 3 minutes. Slides were sealed with Vectashield Antifade Mounting Medium (Vector Laboratories). For DAB immunoprecipitation and antigen detection, samples were blocked with 10% goat serum for 1 h after which they were incubated with primary antibody listed in **Supplementary table 2** at 4˚C overnight. Next day, slides were triple washed with 0.1% Triton-X in PBS and incubated with 1:1000 biotinylated anti-rabbit antibody (Dako) for 2 hours at RT, triple washed. Immunoreactivity was visualized using DAB (0.4 mg/ml, Sigma-Aldrich) as a chromogen. After a dehydration series, stained sections were mounted with DPX (Sigma-Aldrich) and visualized with a light microscope (Leica Microsystems).

Stereological and image quantification

The number of TH-positive cells in the SN was determined by stereological measurements using the Optical fractionator method as described before[19] (StereoInvestigator; MicroBrightField, Magdeburg, Germany). Every fourth section throughout the SN was analyzed, with a total of 6 sections for each animal. The coefficient of error calculated according to the procedure of Schmitz and Hof (Schmitz and Hof, 2005), varied between 0.05 and 0.10. For the fluorescent triple stereological quantifications, we performed similar stereological measurements, using the same parameters mentioned above but we made use of the software Stereologer®, SRC Biosciences (Stereology Resource Center, Inc.). We quantified both the injected and non-injected SN (internal control). An investigator blinded to the

different groups performed all the analyses. For image quantifications we used FIJI software. For fluorescent analyses, we quantified the Mean Fluorescent Intensity (MFI) or the % positive area after adaptive and unbiased thresholding. Threshold was set automatically using either Yen or Triangle threshold. In this case we outline the area of interest and quantify the MFI or percentage of positive area after threshold.

Spectral analysis of conformational variants *in vivo*

The emission spectra of h-FTAA were analyzed by confocal microscopy (Zeiss LSM 880). Cell-specific h-FTAA positive intracellular inclusions were analyzed with neuronal (NeuN), astrocytic (GFAP), microglial (Iba-1) or oligodendroglial (Olig2) markers to determine the cell type of the inclusion. For each condition, 6 different areas in striatum or corpus callosum were scanned at 40x magnification. A minimum of 100 cells were analyzed with the emitted spectrum collected from 7 animals of each experimental group or 5 MSA patients and control subjects. Spectra were normalized to fluorescence peak intensity and the relative peak intensity at 520 and 600 nm were used to quantify the conformational state of h-FTAA-positive inclusions.

Spectral analysis of αSyn assemblies *in vitro*

αSyn fibrils and ribbons were generated as previously described[16] and diluted to 70 μM in PBS (10 mM phosphate, 140 mM NaCl, 2.7 mM KCl, pH 7.4). The LCO h-FTAA was added to the samples at a final concentration of 600 nM, and the emission spectrum of the ligand bound to αSyn fibrils or ribbons was collected using a Tecan Infinite M1000 Pro plate reader (Tecan) exciting h-FTAA at 480 nm. Monomeric αSyn was included as a negative control.

Statistical analysis

Statistical analysis was performed using GraphPad Prism 9 software. The type of analysis with post hoc correction for multiple testing is indicated in the legend of each figure. Statistical levels were set at *p <0.05, **p<0.01, ***p<0.001.

Data availability

The data that support the findings of this study are available from the corresponding authors, upon reasonable request.

Results

Transgenic PLP-αSyn mice (from here on referred to as 'MSA mice') express human αSyn in oligodendrocytes and typically start showing αSyn-rich deposits as early as at 2 months old.[15] Smaller inclusions, that might represent oligomeric species of αSyn, develop in neurons, astrocytes and microglial cells but never to the same extent as the accumulation of aggresomal, GCI-like structures in oligodendrocytes. Neuroinflammation, characterized by microglial activation, is one of the earliest features that develop in these MSA mice together with non-motor features that include loss of neurogenic control of the urinary bladder[20] and REM sleep behavior disorder[21]. Autonomic features precede dopaminergic cell loss and motor deficits by several months, which subsequently deteriorate in a progressive manner.[15] Myelin loss is not typically found, suggesting that in this model demyelination is one of the latest features and that it follows neuroinflammation and neurodegeneration at later stages.

The MSA mouse model represents thus several of the clinical features of multiple system atrophy, and more specifically the parkinsonian form (MSA-P). These MSA mice exhibit many symptoms that occur during both prodromal and late stages of the disease as a result of oligodendrocytes and neurons distress. The model is therefore well suited to assess whether αSyn strains might affect disease progression in this unique cellular environment. We unilaterally injected 2 µl, containing 5 µg, of the αSyn strains fibrils or ribbons (**Supplementary Fig. 1**) in the dorsal striatum of 5 months old MSA mice. As a control group, we injected 2 µl of BSA at a similar concentration. We allowed the MSA mice to age for 9 months after injection and subjected them to different behavioral tests at 6 and 9 months post injection (p.i.). At 6 months p.i., we did not observe any significant behavioral changes between the different groups injected with the two strains or the control condition (**Fig. 1a, b**). However, at 9 months p.i., we detected a significant worsening in the pole test in MSA mice injected with fibrils compared to the ribbons and control groups (**Fig. 1a, b**). Fibrils injected MSA mice took significantly longer to turn and descend during the pole test (**Fig. 1b**). The same conclusion was observed 9 months p.i. using the cylinder test indicating progressive worsening of motor symptoms upon fibrils injection (**Fig. 1c**).

It has been shown that motor changes assessed by the pole and cylinder tests reflect neurodegenerative events in the striatonigral pathway. We therefore assessed via stereological quantifications if fibrils could accelerate dopaminergic cell loss in substantia nigra pars compacta (SNpc). Compared to the BSA control condition, we found that fibrils caused a significant reduction of tyrosine hydroxylase (TH^+)-positive cells (**Fig. 1d**). Fibrils worsened pathology by 35%, whereas ribbons caused a non-significant reduction of TH cells by 17%. Fibrils also induced a significant loss of medium spiny neurons ($DARPP\text{-}32^+$ cells) in the striatum (**Fig. 1e**) further reflected by a loss of neuronal cells ($NeuN^+$ cells) (**Fig. 1f**). The neurotoxicity of fibrils was accompanied by a striking reduction of fluoromyelin signal throughout the striatum (**Fig. 1g**). The strong loss of myelin was also apparent by severe brain atrophy and ventricle enlargement. Fibrils but not ribbons or BSA caused loss of striatal volume of 1.6 mm^3 (**Fig. 1h**), corresponding with a ventricular enlargement of 1.4 mm^3 (**Fig. 1i, 1j)**.

To further characterize the pathological accumulation of αSyn, we performed staining for pSer129-αSyn in combination with the conformation sensitive luminescent conjugated oligothiophene (LCO) h-FTAA.[18] Since pSer129-αSyn does not strictly represent an aggregated state of αSyn, this fluorescent probe can identify specific fibrillar αSyn assemblies. First, to test if h-FTAA binds glial cytoplasmic inclusions in human brain, we performed double labeling of pSer129-αSyn with h-FTAA in the putamen of multiple system atrophy patients (**Fig. 2a, b**). In control subjects, we detected no pSer129-αSyn deposits and no h-FTAA signal. However, in multiple system atrophy brain, we found widespread pSer129-αSyn positive cells that extensively overlap with h-FTAA, showing that the probe can detect GCIs in human brain tissue (**Fig. 2d, e**). Interestingly, when performing pSer129-αSyn and h-FTAA double staining on tissue of BSA-injected MSA mice, we detected pSer129-αSyn positive cells but in large absence of h-FTAA (**Fig. 2c**). Small, intra- or subcellular oligodendroglial inclusions could be detected in these control animals, but these punctate inclusions were sparse (**Fig. 2d, e and Supplementary Fig 2**). This contrasts with animals injected with the two strains where we detected $pSer129\text{-}\alpha Syn^+/h\text{-}FTAA^+$ double positive cells throughout the injected area. Injection of ribbons and fibrils resulted in a significantly increased number of pSer129-αSyn (**Fig. 2f**) and h-FTAA (**Fig. 2g**) inclusions with approximately 25% of double positive $pSer129\text{-}\alpha Syn^+/h\text{-}FTAA^+$ cells in both conditions (**Fig. 2h**). This indicates that in the control MSA mice, pSer129-αSyn is mostly in a non-aggregated state, whereas after injection and seeding with ribbons and fibrils, αSyn pathology changes with the appearance of insoluble pSer129-αSyn inclusions. In addition, fibrils injected in the striatum also induced pSer129-αSyn positive neuritic inclusions formation in dopaminergic neurons in the SN, whereas ribbons did not **(Supplementary Fig. 3).**

The detection of h-FTAA$^+$ inclusions after injection of ribbons and fibrils as opposed to the low signal in control MSA mice is indicative of active seeding by ribbons and fibrils in this model. To examine if ribbons and fibrils can differentially imprint their structure within this environment, we further analyzed the fluorescent emission spectrum of the conformation-sensitive probe h-FTAA. By labeling different cells with cell type specific markers, we could identify h-FTAA$^+$ inclusions in oligodendrocytes, neurons, microglia and astrocytes (**Fig. 3a-c**). From oligodendroglia-positive inclusions we measured the relative fluorescent emission spectrum (**Fig. 3d**). The relative emission spectra of oligodendroglial inclusions, indicative of their conformational state, differed significantly between the three experimental conditions (**Fig. 3e**). Inclusions in oligodendroglia from the BSA-injected MSA mice showed a highly heterogeneous conformational state, reflected by the high variability of assemblies detected. Fibrils caused a significant change in the aggregate conformation whereas ribbons showed a narrower distribution that most closely resembled that of multiple system atrophy patients (**Fig. 3e**). This shows that fibrils and ribbons restrict the conformational landscape and yield different conformational states in oligodendrocytes in a strain-dependent manner. The conformational landscape in neurons, measured via the relative h-FTAA emission spectra (**Fig. 3f**), shows that fibrils and ribbons also yield aggregates with different conformations in neurons (**Fig. 3g**), and to a lesser extent in microglia (**Fig. 3h, i**), while no differences were detected in astrocytes. (**Fig. 3j, k**). Collectively, these results show that αSyn ribbons and fibrils with strain-specific pathology have unique seeding capacities in distinct cellular environments.

To further evaluate the pathogenicity of the two strains, we assessed if different strains of αSyn can induce immune changes in MSA mice. Inflammation or microglial activation have been shown to be early events in this *in vivo* model.[15] It is described that different strains of αSyn, including fibrils and ribbons, can elicit a macrophagic response in human monocytes and that this might be strain-dependent.[22] High molecular weight species of αSyn bind to TLR2 and TLR4 receptors, which recognize pathogen-associated patterns, causing glia to become active and produce pro-inflammatory cytokines.[23–25] In our MSA transgenic mice, TLR4 is upregulated[26] and microglial cells change from a homeostatic to an active state with the release of pro-inflammatory markers before any detectable neurodegenerative changes have occurred.[15] It is not exactly known what the role of macrophagic cells is during the neurodegenerative process, but it is suggested that activated microglial cells might aggravate multiple system atrophy pathology through the release of pro-inflammatory cytokines in addition to clearing pathogenic αSyn strains through the establishment of F-actin dependent intermicroglia networks.[25,27] We therefore examined the effects of αSyn strains on the microglial

immune response *in vivo* and *in vitro*. Via staining of Iba-1 in combination with the lysosomal marker CD68 for activated microglia we observed strong Iba-1 and CD68 expression in both the fibrils and ribbons conditions at 9 months post injection (**Fig. 4a-c)**. Microglial cells were ramified and phagocytic with no clear differences in Iba-1 expression between the two conditions (**Fig. 4a-b**). In contrast, we found that microglial cells were significantly more active in the fibrils condition, as indicated by stronger CD68 staining, whereas this was much less apparent in the ribbons condition (**Fig. 4c**). Microglial cells were sometimes found to engulf cell debris or pSer129-αSyn inclusions **(Fig. 4d)** and were furthermore MHCII-positive, especially in the fibril condition (**Fig. 4e,f**) indicating that fibrils are potentially recognized as pathogens and that they can trigger antigen presentation by resident brain macrophages as recently reported for astrocytes.[28]

To better characterize the microglial inflammatory response with respect to the different recombinant αSyn strains, we extended our analysis to primary mouse microglia *in vitro*. We administered the two different strains of αSyn to primary murine microglia cultures. Treatment with BSA was used as a negative control. In order to assess uptake of different αSyn assemblies, we performed immunocytochemistry for αSyn and the microglial marker Iba1 at 24 hours after administration. αSyn ribbons and fibrils co-localized with primary microglial cells (**Fig. 5a)**. Microglial pro-inflammatory response in reaction to different αSyn assemblies was further examined. The expression levels of pro-inflammatory markers TNFα, IL1β and IL6 were strongly upregulated upon administration of αSyn fibrils and to a lesser extent for ribbons (**Fig. 5b-d**). This again shows that αSyn strains, and more specifically αSyn fibrils, can act as a direct inflammatory trigger and that the structure of the assembly type is crucial for triggering the immune response.

Next to microglial cells, astrocytes take part in the innate immune response and also express different types of TLRs that recognize misfolded αSyn.[24,27] Extensive astrocytic activation is apparent during post-mortem examination of human multiple system atrophy brain but is generally absent in the MSA mouse model, suggesting that astrocytic activation might represent an event that occurs at later stages or that the MSA model might require an additional trigger to activate astrocytic response. Astrocytes take up misfolded αSyn via endocytosis as they try to degrade toxic protein via the lysosomal pathway.[28–30] Unsuccessful clearance of high molecular weight assemblies can sometimes result in protein accumulation and in multiple system atrophy brain, astrocytic inclusions have been described in the brain stem and the cerebellum of multiple system atrophy patients whereas others have described a lack of inclusions in protoplasmic astrocytic in putamen and substantia nigra.[31,32] It is not known if this

could reflect a loss of astrocytes after αSyn uptake and pathological accumulation, or the absence inclusions in reactive astrocytes in these areas. After injecting ribbons and fibrils in the striatum, we found that both strains caused a strong increase of GFAP markers (**Fig. 6a-c**). Interestingly, even though fibrils were most toxic in MSA mice, they did not cause more astrocytic activation in the striatum compared to ribbons. In the ribbon condition, we detected a higher number of pSer129-αSyn inclusions in astrocytes in the striatum, which was in large contrast to fibrils where significantly fewer inclusions were detected **(Fig. 6b, d**). We tested if these inclusions were aggregated assemblies by staining with h-FTAA and GFAP and found that astrocytes indeed accumulate aggregated αSyn (**Fig. 4b**). This indicates that astrocytes can take up αSyn strains but also accumulate pathogenic species probably as a result of strain exposure or phagocytosis of dying cell debris.

Reactive astrocytes and microglia can upregulate cytokine production and release pro-inflammatory mediators that cause neuronal and oligodendroglial damage. Such a pro-inflammatory state could potentially perpetuate the toxicity of αSyn via central but also peripheral immune cells.[33] To determine whether the Iba-1 cells were resident brain microglial cells, we co-stained for the microgial marker TMEM119 ($Iba1^+/Tmem119^+$), which is absent in peripheral macrophages ($Iba1^+/Tmem119^-$).[34] Surprisingly, we found significantly higher numbers of non-resident macrophages ($Iba1^+Tmem119^-$) in animals injected with ribbons and fibrils (**Fig. 7a, b**). To further investigate the potential contribution of peripheral cells, we stained for CD45, a marker highly expressed in peripheral myeloid and leukocytic cells but with low expression in microglial cells. In the atrophied striatum after injection with fibrils, we found CD45 positive cells throughout the affected area but more abundantly around the lateral ventricles and blood vessels indicating that peripheral immune cells have infiltrated the affected area via these sites (**Fig 7c, d).** This effect was much less pronounced in the ribbons condition and was absent in the BSA control condition (**Fig. 7c)**. Since we observed that in response to αSyn ribbons and fibrils glial cells became phagocytic and antigen presenting, we next asked how this might influence the recruitment of T cells. Both in the fibrils and ribbons condition we detected positive staining for CD3 (**Fig. 7 k**)**e, f**) suggesting that in conjunction with the presence of MHCII-positive cells T cells might aid microglial cells in the recognition and the clearance of pathogenic species of αSyn. CD3 positive T cells were found throughout the striatum and much more abundant in the case of fibrils compared to ribbons, whereas we did not find any positive cells in the control animals injected with BSA (**Fig. 7e**).

Discussion

Recent studies have shown that αSyn strains might play an important role in multiple system atrophy etiopathogenesis. Through their unique conformation, αSyn strains can cause multiple system atrophy-like features in cells and *in vivo.*[9,17] Oligodendrocytes offer a unique intracellular environment in which monomeric αSyn forms highly infectious and toxic high molecular weight assemblies.[6] The evidence for a role of strains in multiple system atrophy pathogenesis has mostly been studied via indirect methods but recently it was shown via cryo-EM that αSyn filaments in the brain of multiple system atrophy patients have defined structural characteristics.[7] Depending on the site of isolation, small variations exist in the structure of the fibril of which the ratio varied between patients.

Multiple system atrophy pathogenic assemblies isolated from human brain, either as a crude homogenate or amplified *in vitro*, cause unique neurodegenerative phenotypes upon injections into animals but interestingly, propagation is dependent on the animal model used.[6,9,14,35–37] To date, all inoculation studies performed with multiple system atrophy strains in WT or transgenic Parkinson's disease mice did not reproduce a robust multiple system atrophy phenotype with significant oligodendroglial pathology. Indeed, we have recently reported that αSyn strains derived from the brain of multiple system atrophy patients, either as crude homogenates or upon amplification *in vitro*, while inducing the most pronounced disease phenotype in a Parkinson's disease model as compared to Parkinson's disease or dementia with Lewy body strains, do not yield oligodendroglial inclusions.[8] There thus appears to be a discrepancy between the disease strain, the host and the disease phenotype and this prompted the question if strains can propagate oligodendrogliopathy.

In this study we therefore assessed whether different αSyn strains can propagate in an multiple system atrophy model and if so, if different multiple system atrophy-like phenotypes, reflective of the multiple disease types in multiple system atrophy, might develop. We injected two extensively characterized αSyn strains, ribbons and fibrils, in a well-established transgenic multiple system atrophy mouse model (PLP- αSyn or MSA mice).[15] We followed disease progression over multiple months by assessing motor behavior. We found that behavioral motor symptoms appeared at 9 months after striatal injections with fibrils, but not with ribbons. Multiple system atrophy mice injected with fibrils showed significant pathology of both nigral and striatal neurons whereas toxicity was limited for the ribbons condition. We also discovered strong demyelination and brain atrophy in relevant disease-associated regions, which previously had only been described in a transgenic multiple system atrophy model based on

overexpression of αSyn by the myelin basic protein promoter.[38] These findings reflect the advanced neuropathology of multiple system atrophy patients with the loss of striatal medium spiny neurons (dopamine receptor expressing) and the loss of nigral neurons (dopamine producing).

We next examined how αSyn pathology develops in the absence or presence of the two αSyn strains. The MSA mouse model is characterized by the expression of αSyn in oligodendrocytes that is post translationally modified at position Ser129. First, we analyzed αSyn pathology in the BSA injected MSA mice and found that pSer129-αSyn positive cells were not positive for the aggregation sensitive probe h-FTAA. Since h-FTAA can bind to early aggregated species not detected by conventional ligands[18], this shows that the majority of αSyn is post translationally modified, likely because of its relatively high intracellular expression levels, but that it does not form high molecular weight species in oligodendrocytes. These immunohistochemical findings were in stark contrast with what we observed in multiple system atrophy patient brain, where pSer129-αSyn^{+} inclusions were co-stained by h-FTAA with nearly perfect overlap between both markers. Previous work showed that sarkosyl insoluble αSyn could be extracted from aged multiple system atrophy transgenic mice with a shift in assembly states detected via Western Blot[15,39]. This could indicate the presence of diffuse or low abundance oligomers that might be undetectable with confocal microscopy or reflect the sparse and punctuate distribution of h-FTAA inclusions in these mice. LCOs have a flexible conformation that reflect in their fluorescent emission profiles[18]. This allows assessing the structural characteristics of the aggregates they bind to. The spectral profiles of h-FTAA positive inclusions revealed that the punctuate pSer129-αSyn-negative inclusions in the MSA mice were heterogeneous. This suggests they are immature without a dominant conformation. In the caudate putamen of multiple system atrophy patients the conformational state of the GCIs appeared more uniform reflecting a much more restricted conformational landscape. After injection of ribbons and fibrils in the mouse striatum, the total number of pSer129-αSyn increased with the detection of pSer129-αSyn^{+}/h-FTAA^{+} double positive inclusions. This increase in the number of cells appeared similar for both ribbons and fibrils. However, the distribution and characteristics of the seeded inclusions differed significantly. Ribbons triggered a conformational profile in oligodendrocytes reminiscent of multiple system atrophy patients, with a narrower h-FTAA positive inclusions spectrum, i.e. restricted assembly state, as compared to that observed for fibrils. Further illustrating the importance of the cellular environment, is that upon incubation of the two αSyn strains with h-FTAA *in vitro*, the emission spectra of the two strain largely overlap (**Supplementary fig. 4**) whereas *in vivo* the spectra of the intracellular inclusion vary significantly. Interestingly, we also reported recently that Parkinson's disease and multiple system atrophy patient-derived αSyn strains obtained by PMCA

significantly resembled ribbons, while those derived from dementia with Lewy body patients resembled fibrils.[8] Therefore, the ability of the two strains to seed pathology with different conformational profiles and associated pathological pattern indicates that the resulting pathology is not a reflection of an accelerated phenotype inherent to the transgenic MSA mouse model but instead that the pathology is the result of a new phenotype that is driven by both the strain conformation and the host background.

These results corroborate our previous work where we showed that αSyn strains can amplify distinct structures with fibrils being the most toxic species *in vivo* and ribbons causing a distinct type of inclusions.[16,17] In this study we found more pSer129-αSyn pathology in astrocytes induced by ribbons compared to fibrils, while in our previous study ribbons also induced sparce pSer129-αSyn pathology in oligodendrocytes. These differences might be due to the chosen injection site (striatum instead of substantia nigra) and/or to the different cellular milieu and αSyn expression levels (transgenic αSyn overexpression in oligodendrocytes vs AAV-vector mediated overexpression in dopaminergic neurons). The reason why fibrils might be more pathogenic than ribbons can be multifold and is likely governed through the exposed strain surfaces that uniquely interact within their environment.[40,41] Along those lines, neuroinflammation has been hypothesized to play an important role in multiple system atrophy. Although its exact role is elusive, microglial activation is considered an early event in multiple system atrophy etiopathogenesis and persists while the disease progresses. In multiple system atrophy animals a microglial response is one of the earliest disease events and administration of minocycline, a microglial polarization and activation inhibitor, can ameliorate multiple system atrophy pathology *in vivo.*[42] Microglial activation accompanies αSyn pathology in human multiple system atrophy brain, not only in late but also in earlier disease stages[43] and PET tracers bind activated microglial cells in putamen and pons of multiple system atrophy patients.[44] To determine whether αSyn strains could modulate inflammation, we exposed primary microglial cells to fibrils or ribbons and observed that both strains differentially interact with microglial cells *in vitro*. In contrast to ribbons, fibrils triggered a strong pro-inflammatory response, with the release of Il-1β, Il-6 and TNF-α. Similarly, we found that *in vivo* exposure of fibrils caused severe inflammation *in vivo* with increased phagocytic activity of microglial cells.[25]

Next to microglial cells, astrocytes can take up αSyn fibrils and target it for lysosomal degradation.[30] Some studies have reported astrocytic inclusions of αSyn in multiple system atrophy, sometimes in advanced stages of the disease. Phosphorylated αSyn inclusions in astrocytes were found in the ventrolateral part of the spinal cord and brainstem[45] whereas another study reported astrocytic

inclusions in the cerebellum[32] but the presence of these inclusions in areas such as the nigra and striatum remain more elusive.[31] Astrocytes can assist in the removal of protein aggregates release from neurons and astrocytes are directly coupled via cell junctions to oligodendrocytes.[46] Since a large proportion of binding receptors for fibrils are unique for astrocytes and do not exist in neurons, this raises the possibility that astrocytes might uniquely assist in the removal of defined αSyn assemblies that are released from oligodendroglia.[47,48] In the injected MSA mice we found astrocytic inclusions of PSer129-αSyn that were much more prominent in the ribbons group. We could speculate that ribbons are taken up more efficiently in astrocytes, or alternatively, that fibrils cause rapid loss of astrocytes. Alternatively, a more efficient sequestration of ribbons in astrocytes or a higher ribbons astrocytic degradation efficacy might further explain why ribbons have lower pathogenicity in this model compared to fibrils.

Our *in vitro* and *in vivo* work therefore shows that αSyn strains can be taken up by different types of glial cells and trigger inflammation. Fibrils elicited strong expression of MHCII receptors on macrophagic cells which is indicative of an active response towards non self-antigens of abnormal αSyn. Pathogenic assemblies can be presented by resident antigen presenting cells to recruit lymphocytes. Alternatively, or additionally, αSyn seeds can be secreted in the extracellular space into the CSF or the glymphatic and lymphatic systems where they can activate lymphocytes and elicit a humoral response in a more systemic manner. It was shown that T-cells can be recruited in a model of experimental multiple system atrophy, which was confirmed in post mortem multiple system atrophy brain tissue.[49] Cytokine profiling from cerebrospinal fluid and brain tissue from patients showed that pro-inflammatory pathways are upregulated.[50–52] Elevated numbers of $CD3^+$ and $CD4^+$ cells have also been found in the periphery during earlier disease stages,[53] and blood transcriptomics showed prominent enrichment of gene sets related to immunity and inflammation.[54] In this study, we now find that αSyn strains can differentially trigger an adaptive immune response resulting in the recruitment of peripheral lymphocytes adding an additional mechanism by which αSyn strains can contribute to multiple system atrophy pathology. Given that multiple system atrophy-specific strains exist in patient brain and cause pathology via multiple mechanisms, targeting these disease-related assemblies via peripheral or central routes could therefore be a valuable therapeutic strategy.

Since strains can propagate oligodendrogliopathy *in vivo* but only in the presence of oligodendroglial αSyn the question now remains how such an environment might arise. Oligodendroglia express relatively low levels of αSyn and impose a protective counter-amplification barrier that preserves their

integrity. It has been proposed that multiple system atrophy could be triggered by an external event but what such a trigger could be is currently unknown.[55,56] In the PLP-αSyn mouse model, external stressors, such as oxidative stress, mitochondrial dysfunction[57] and proteasome disruption,[58] contributed to pathology. Infections can transiently impair protein clearance and trigger αSyn aggregation in vivo.[59] Host genetic susceptibility and exogenous or environmental triggers might be more closely related than previously appreciated and immune triggers could have such a role as multiple system atrophy patients often experience frequent infections in the gut, lungs or urinary tract.[60–62] An altered humoral response has been described in Parkinson's disease via association of MHC alleles, which confers increased disease risk.[51,63] Peptides of post-translationally modified αSyn can elicit an unwanted response from cytotoxic and helper T-cells in Parkinson's disease patients that are recognized by specific MHC alleles.[64] This work now suggests that the innate and adaptive immune systems can be involved in multiple system atrophy pathogenesis via exposure to αSyn strains. Further investigation will need to establish whether an HLA haplotype might exist for multiple system atrophy and whether disease relevant strains derived from multiple system atrophy brain could aggravate disease differently, as opposed to Parkinson's disease strains.

In conclusion, this study demonstrates that multiple system atrophy is the consequence of an interaction between defined αSyn strains and cellular environments. Our data also show that injection of αSyn strains can trigger oligodendrogliopathy and neuronal pathology with inflammation thus yielding a unique animal model that more closely mimics the human multiple system atrophy condition.

Acknowledgements

We thank T. Bellande for expert technical assistance and L. Bousset for advice in αSyn strains preparation. We acknowledge the NeuroBiobank of the Born-Bunge Institute, Wilrijk (Antwerpen), Belgium; ID: BB190113 for providing MSA patient and control brain tissue.

Funding

This work was supported by the FWO Flanders (Projects G.0927.14), the KU Leuven (OT/14/120, C14/18/102), the 2017 and 2020 JiePie MSA-AMS awards to V.B. and W.P., the Flemish Parkinson Liga

(VPL) and Fund Sophia managed by the King Baudouin Foundation. W.P. acknowledges a post-doctoral fellowship from Fulbright, IDT Technologies and FWO Flanders. N.S. acknowledges a grant of the Austrian Science Fund (FWF) F4414. R.M. acknowledges support through the JiePie 2019 award. R.M. and A.C. received funding from the EC Joint Programme on Neurodegenerative Diseases (TransPathND, ANR-17-JPCD-0002-02) and the Innovative Medicines Initiative 2 Joint Undertaking under grant agreement No 116060 (IMPRiND). This Joint Undertaking receives support from the European Union's Horizon 2020 research and innovation programme and EFPIA with support by the Swiss State Secretariat for Education, Research and Innovation (SERI) under contract number 17.00038. The Confocal Images were recorded on a Zeiss LSM 880—Airyscan (Cell and Tissue Imaging Cluster (CIC), Supported by Hercules AKUL/15/37_GOH1816N and FWO G.0929.15 to Pieter Vanden Berghe, KU Leuven).

Competing interests

The authors report no competing interests.

Supplementary material

Supplementary material is available at *Brain* online.

References

1. Fanciulli A, Wenning GK. Multiple-System Atrophy. *N Engl J Med*. 2015;372(3):249-263. doi:10.1056/NEJMra1311488

2. Krismer F, Wenning GK. Multiple system atrophy: insights into a rare and debilitating movement disorder. *Nat Publ Gr*. Published online March 2017:1-12. doi:10.1038/nrneurol.2017.26

3. Palma J-A, Norcliffe-Kaufmann L, Kaufmann H. Diagnosis of multiple system atrophy. doi:10.1016/j.autneu.2017.10.007

4. Wenning GK, Geser F, Krismer F, et al. The natural history of multiple system atrophy: a prospective European cohort study. *Lancet Neurol*. 2013;12(3):264-274. doi:10.1016/S1474-4422(12)70327-7

5. Grazia Spillantini M, Anthony Crowther R, Jakes R, Cairns NJ, Lantos PL, Goedert M. Filamentous α-synuclein inclusions link multiple system atrophy with Parkinson's disease and dementia with Lewy bodies. *Neurosci Lett*. Published online 1998. doi:10.1016/S0304-3940(98)00504-7

6. Peng C, Gathagan RJ, Covell DJ, et al. Cellular milieu imparts distinct pathological α-synuclein strains in α-synucleinopathies. *Nature*. Published online 2018. doi:10.1038/s41586-018-0104-4

7. Schweighauser M, Shi Y, Tarutani A, et al. Structures of α-synuclein filaments from multiple system atrophy. doi:10.1038/s41586-020-2317-6

8. Van Der Perren A, Gelders G, Fenyi A, Bousset L, Brito F, Peelaerts W. The structural differences between patient - derived α - synuclein strains dictate characteristics of Parkinson ' s disease , multiple system atrophy and dementia with Lewy bodies. *Acta Neuropathol*. 2020;139(0123456789):977-1000.

9. Prusiner SB, Woerman AL, Mordes DA, et al. Evidence for α-synuclein prions causing multiple system atrophy in humans with parkinsonism. *Proc Natl Acad Sci U S A*. 2015;112(38):E5308-E5317. doi:10.1073/pnas.1514475112

10. Shahnawaz M, Mukherjee A, Pritzkow S, et al. Discriminating α-synuclein strains in Parkinson's disease and multiple system atrophy. *Nature*. Published online February 2020.

doi:10.1038/s41586-020-1984-7

11. Yamasaki TR, Holmes BB, Furman JL, et al. Parkinson's disease and multiple system atrophy have distinct -synuclein seed characteristics. *J Biol Chem*. 2019;294(3):1045-1058. doi:10.1074/jbc.RA118.004471

12. Collinge J. Mammalian prions and their wider relevance in neurodegenerative diseases. *Nature*. 2016;539(7628):217-226. doi:10.1038/nature20415

13. Li J, Browning S, Mahal SP, Oelschlegel AM, Weissmann C. Darwinian Evolution of Prions in Cell Culture. *Science (80-)*. 2010;327(5967):869-872. doi:10.1126/SCIENCE.1183218

14. Marmion D, Peelaerts W, Kordower J. A historical review of multiple system atrophy with a critical appraisal of cellular and animal models. *J Neural Transm*. 2021;128(10):1507-1527. doi:10.1007/S00702-021-02419-8

15. Refolo V, Bez F, Polissidis A, et al. Progressive striatonigral degeneration in a transgenic mouse model of multiple system atrophy: translational implications for interventional therapies. *Acta Neuropathol Commun*. 2018;6(1):1-24. doi:10.1186/s40478-017-0504-y

16. Bousset L, Pieri L, Ruiz-Arlandis G, et al. Structural and functional characterization of two alpha-synuclein strains. *Nat Commun*. 2013;4:2575. doi:10.1038/ncomms3575

17. Peelaerts W, Bousset L, Van Der Perren A, et al. α-Synuclein strains cause distinct synucleinopathies after local and systemic administration. *Nature*. Published online 2015. doi:10.1038/nature14547

18. Klingstedt T, Åslund A, Simon RA, et al. Synthesis of a library of oligothiophenes and their utilization as fluorescent ligands for spectral assignment of protein aggregates. *Org Biomol Chem*. 2011;9(24):8325-8356. doi:10.1039/c1ob05637a

19. Baekelandt V, Claeys A, Eggermont K, et al. Characterization of Lentiviral Vector-Mediated Gene Transfer in Adult Mouse Brain. *Hum Gene Ther*. 2002;13(7):841-853. doi:10.1089/10430340252899019

20. Boudes M, Uvin P, Pinto S, et al. Bladder dysfunction in a transgenic mouse model of multiple system atrophy. *Mov Disord*. 2013;28(3):347-355. doi:10.1002/mds.25336

21. Härtner L, Keil TWM, Kreuzer M, et al. Distinct parameters in the EEG of the PLP α-SYN mouse model for multiple system atrophy reinforce face validity. *Front Behav Neurosci*. 2017;10. doi:10.3389/FNBEH.2016.00252

22. Grozdanov V, Bliederhaeuser C, Ruf WP, et al. Inflammatory dysregulation of blood monocytes in Parkinson's disease patients. *Acta Neuropathol*. 2014;128(5):651-663. doi:10.1007/s00401-014-1345-4

23. Kim C, Ho DH, Suk JE, et al. Neuron-released oligomeric α-synuclein is an endogenous agonist of TLR2 for paracrine activation of microglia. *Science (80-)*. 2013;353(6307). doi:10.1038/ncomms2534

24. Fellner L, Irschick R, Schanda K, et al. Toll-like receptor 4 is required for α-synuclein dependent activation of microglia and astroglia. *Glia*. 2013;61(3):349-360. doi:10.1002/glia.22437

25. Scheiblich H, Bousset L, Schwartz S, et al. Microglial NLRP3 Inflammasome Activation upon TLR2 and TLR5 Ligation by Distinct α-Synuclein Assemblies. *J Immunol*. 2021;207(8):2143-2154. doi:10.4049/jimmunol.2100035

26. Dehay B, Martinez-Vicente M, Ramirez A, et al. Lysosomal dysfunction in Parkinson disease. *Autophagy*. 2012;8(9):1389-1391. doi:10.4161/auto.21011

27. Stefanova N, Fellner L, Reindl M, Masliah E, Poewe W, Wenning GK. Toll-Like Receptor 4 Promotes-Synuclein Clearance and Survival of Nigral Dopaminergic Neurons. *Am J Pathol*. 2011;179:954-963. doi:10.1016/j.ajpath.2011.04.013

28. Russ K, Teku G, Vihinen M, Melki R, Correspondence LR. TNF-a and a-synuclein fibrils differently regulate human astrocyte immune reactivity and impair mitochondrial respiration. *Cell Rep*. 2021;34. doi:10.1016/j.celrep.2021.108895

29. Rostami J, Holmqvist S, Lindström V, et al. Human Astrocytes Transfer Aggregated Alpha-Synuclein via Tunneling Nanotubes. *J Neurosci*. 2017;37(49):11835-11853. doi:10.1523/JNEUROSCI.0983-17.2017

30. Loria F, Vargas JY, Bousset L, et al. α-Synuclein transfer between neurons and astrocytes indicates that astrocytes play a role in degradation rather than in spreading. *Acta Neuropathol*. 2017;134(5):789-808. doi:10.1007/S00401-017-1746-2/FIGURES/9

31. Song YJC, Halliday GM, Holton JL, et al. Degeneration in different parkinsonian syndromes relates to astrocyte type and astrocyte protein expression. *J Neuropathol Exp Neurol*. 2009;68(10):1073-1083. doi:10.1097/NEN.0b013e3181b66f1b

32. Piao YS, Mori F, Hayashi S, et al. α-Synuclein pathology affecting Bergmann glia of the cerebellum in patients with α-synucleinopathies. *Acta Neuropathol*. 2003;105(4):403-409. doi:10.1007/s00401-002-0655-0

33. Peralta Ramos JM, Iribarren P, Bousset L, Melki R, Baekelandt V, Van der Perren A. Peripheral inflammation regulates CNS immune surveillance through the recruitment of inflammatory monocytes upon systemic α-synuclein administration. *Front Immunol*. 2019;10(JAN):1-6. doi:10.3389/fimmu.2019.00080

34. Bennett ML, Bennett FC, Liddelow SA, et al. New tools for studying microglia in the mouse and human CNS. *Proc Natl Acad Sci U S A*. 2016;113(12):E1738--46. doi:10.1073/pnas.1525528113

35. Woerman AL, Oehler A, Kazmi SA, et al. Multiple system atrophy prions retain strain specificity after serial propagation in two different Tg(SNCA*A53T) mouse lines. *Acta Neuropathol*. 2019;137(3):437-454. doi:10.1007/s00401-019-01959-4

36. Sargent D, Verchère J, Lazizzera C, et al. 'Prion-like' propagation of the synucleinopathy of M83 transgenic mice depends on the mouse genotype and type of inoculum. *J Neurochem*. 2017;143(1):126-135. doi:10.1111/jnc.14139

37. Bernis ME, Babila JT, Breid S, Wüsten KA, Wüllner U, Tamgüney G. Prion-like propagation of human brain-derived alpha-synuclein in transgenic mice expressing human wild-type alpha-synuclein. *Acta Neuropathol Commun*. Published online November 2015:1-18. doi:10.1186/s40478-015-0254-7

38. May VEL, Ettle B, Poehler A-M, et al. $α$-Synuclein impairs oligodendrocyte progenitor maturation in multiple system atrophy. *Neurobiol Aging*. 2014;35(10):2357-2368. doi:10.1016/j.neurobiolaging.2014.02.028

39. Heras-Garvin A, Stefanova N. MSA: From basic mechanisms to experimental therapeutics. *Park Relat Disord*. Published online 2020:1-11.

40. Melki R. How the shapes of seeds can influence pathology. *Neurobiol Dis*. 2018;109:201-208.

doi:10.1016/j.nbd.2017.03.011

41. Shrivastava AN, Bousset L, Renner M, et al. Differential Membrane Binding and Seeding of Distinct α-Synuclein Fibrillar Polymorphs. *Biophys J*. 2020;118(6):1301-1320. doi:10.1016/J.BPJ.2020.01.022

42. Stefanova N, Reindl M, Neumann M, Kahle PJ, Poewe W, Wenning GK. Microglial activation mediates neurodegeneration related to oligodendroglial $α$-synucleinopathy: Implications for multiple system atrophy. *Mov Disord*. 2007;22(15):2196-2203. doi:10.1002/mds.21671

43. Ishizawa K, Komori T, Sasaki S, Arai N, Mizutani T, Hirose T. Microglial activation parellels system degeneration in Multiple System Atrophy. *J Neuropathol Exp Neurol*. 2004;63(1):43-52.

44. Kübler D, Wächter T, Cabanel N, et al. Widespread microglial activation in multiple system atrophy. *Mov Disord*. 2019;14:5-9. doi:10.1002/mds.27620

45. Nakamura K, Mori F, Kon T, et al. Accumulation of phosphorylated α-synuclein in subpial and periventricular astrocytes in multiple system atrophy of long duration. *Neuropathology*. 2016;36(2):157-167. doi:10.1111/neup.12243

46. Orthmann-murphy JL, Abrams CK, Scherer SS. Gap junctions couple astrocytes and oligodendrocytes. *J mol neurosci*. 2009;35(1):101-116. doi:10.1007/s12031-007-9027-5.Gap

47. Shrivastava AN, Redeker V, Fritz N, et al. α-synuclein assemblies sequester neuronal α3-Na + /K + - ATP ase and impair Na + gradient. *EMBO J*. 2015;34(19):2408-2423. doi:10.15252/embj.201591397

48. Shrivastava AN, Redeker V, Fritz N, et al. Data in support of the identification of neuronal and astrocyte proteins interacting with extracellularly applied oligomeric and fibrillar α-synuclein assemblies by mass spectrometry. *Data Br*. 2016;7:221-228. doi:10.1016/j.dib.2016.02.018

49. Williams GP, Marmion DJ, Schonhoff AM, et al. T cell infiltration in both human multiple system atrophy and a novel mouse model of the disease. *Acta Neuropathol*. Published online 2020.

50. Rydbirk R, Elfving B, Andersen MD, et al. Cytokine profiling in the prefrontal cortex of Parkinson's Disease and Multiple System Atrophy patients. *Neurobiol Dis*. 2017;106(C):269-278. doi:10.1016/j.nbd.2017.07.014

51. Yamasaki R, Yamaguchi H, Matsushita T, Fujii T, Hiwatashi A, Kira J ichi. Early strong intrathecal inflammation in cerebellar type multiple system atrophy by cerebrospinal fluid cytokine/chemokine profiles: A case control study. *J Neuroinflammation*. 2017;14(1):89. doi:10.1186/s12974-017-0863-0

52. Li F, Ayaki T, Maki T, Sawamoto N, Takahashi R. NLRP3 Inflammasome-Related Proteins Are Upregulated in the Putamen of Patients With Multiple System Atrophy. *J Neuropathol Exp Neurol*. 2018;77(11):1050-1065. doi:doi: 10.1093/jnen/nly090

53. Cao B, Chen X, Zhang L, et al. Elevated Percentage of CD3+ T-Cells and CD4+/CD8+ Ratios in Multiple System Atrophy Patients. *Front Neurol*. 2020;0:658. doi:10.3389/FNEUR.2020.00658

54. Pérez-Soriano A, Arnal Segura M, Botta-Orfila T, et al. Transcriptomic differences in MSA clinical variants. *Sci Rep*. 2020;10(1). doi:10.1038/S41598-020-66221-4

55. Wenning GK, Stefanova N, Jellinger KA, Poewe W, Schlossmacher MG. Multiple system atrophy: A primary oligodendrogliopathy. *Ann Neurol*. 2008;64(3):239-246. doi:10.1002/ana.21465

56. Johnson ME, Stecher B, Labrie V, Brundin L, Brundin P. Triggers, Facilitators, and Aggravators: Redefining Parkinson's Disease Pathogenesis. *Trends Neurosci*. 2019;42(1):4-13. doi:10.1016/j.tins.2018.09.007

57. Stefanova N, Reindl M, Neumann M, et al. Oxidative stress in transgenic mice with oligodendroglial alpha-synuclein overexpression replicates the characteristic neuropathology of multiple system atrophy. *Am J Pathol*. 2005;166(3):869-876. doi:10.1016/S0002-9440(10)62307-3

58. Stefanova N, Kaufmann WA, Humpel C, Poewe W, Wenning GK. Systemic proteasome inhibition triggers neurodegeneration in a transgenic mouse model expressing human α-synuclein under oligodendrocyte promoter: Implications for multiple system atrophy. *Acta Neuropathol*. 2012;124(1):51-65. doi:10.1007/S00401-012-0977-5

59. Marreiros R, Müller-Schiffmann A, Bader V, et al. Viral capsid assembly as a model for protein aggregation diseases: Active processes catalyzed by cellular assembly machines comprising novel drug targets. *Virus Res*. 2015;207:155-164. doi:10.1016/J.VIRUSRES.2014.10.003

60. Wenning GK, Jecmenica-Lukic M, Poewe W, Tolosa E. Premotor signs and symptoms of multiple

system atrophy. *Lancet Neurol*. 2012;11:361-368.

61. Engen PA, Dodiya HB, Naqib A, et al. The Potential Role of Gut-Derived Inflammation in Multiple System Atrophy. *J Parkinsons Dis*. 2019;7(2):331-346. doi:10.3233/JPD-160991

62. Villumsen M, Aznar S, Pakkenberg B, Jess T, Brudek T. Inflammatory bowel disease increases the risk of Parkinson's disease: a Danish nationwide cohort study 1977-2014. *Gut*. 2019;68(1):18-24. doi:10.1136/gutjnl-2017-315666

63. Rydbirk R, Elfving B, Andersen MD, et al. Cytokine profiling in the prefrontal cortex of Parkinson's Disease and Multiple System Atrophy patients. *Neurobiol Dis*. 2017;106:269-278. doi:10.1016/j.nbd.2017.07.014

64. Sulzer D, Alcalay RN, Garretti F, et al. T cells from patients with Parkinson's disease recognize α-synuclein peptides. *Nature*. 2017;546(7660):656-661. doi:10.1038/nature22815

Figures

Figure 1. αSyn strains cause distinct behavioral and neuronal pathology with demyelination and brain atrophy in MSA mice. Transgenic PLP- αSyn mice injected with fibrils, not BSA or ribbons, present progressive motor deficits 9 months post injection (p.i.). (**A)** Fine motor skills were assessed by the pole test and the time for animals to climb down the pole and **(B)** time to turn (*n* = 7-12, mean ± s.e.m., two-way ANOVA with Tukey's correction for multiple testing, **P* < 0.05, ** < 0.01). **(C)** Detection of unilateral motor deficits using the cylinder test at 9 p.i. shows a decrease in motor behavior for the fibril condition (*n* = 7-12, mean ± s.e.m., t and Wilcoxon test against a hypothetical mean of 50% with Bonferroni correction for multiple testing, **P* < 0.05). **(D)** Neurodegeneration is also more prominent in the fibrillar condition with significant TH^+ cell loss in the substantia nigra compared to control MSA mice (*n* = 7-12, mean ± s.e.m., one-way ANOVA with Tukey's correction for multiple testing, **P* < 0.05)**.** Fibrils cause significant loss of **(E)** striatal medium spiny neurons (DARPP-32) and **(F)** neurons (NeuN) measured by a loss of total number of cells in a coronal section of the anterior striatum (*n* = 7-12, mean ± s.e.m., one-way ANOVA with Tukey's correction for multiple testing, ***P* < 0.01 and ****P* < 0.001). Oligodendrogliopathy was assessed by measuring myelination in the striatum of MSA mice. **(G)** Animals injected with fibrils exhibit severe oligodendroglial pathology whereas animals injected with ribbons or BSA do not (*n* = 7-12, mean ± s.e.m., two-way ANOVA with Tukey's multiple comparison test, *** *P* < 0.001). Note the absence of fluoromyelin signal in the corpus collosum and striatum in the fibril condition. Oligodendroglial- and neuropathology in response to the fibrillar strain is further shown by brain atrophy of the **(H)** striatum and **(I)** ventricular enlargement measured (*n* = 7-12, mean ± s.e.m., two-way ANOVA with Tukey's multiple comparison test, *** *P* < 0.001). **(J)** Representative images showing the extent of brain atrophy and myelin loss in MSA mice injected with BSA, ribbons or fibrils.

Figure 2. αSyn strains-induced h-FTAA-positive inclusions *in vivo*. (A) Detection of αSyn deposits in the putamen of a healthy individual and an MSA patient. Staining for pSer129-αSyn shows widespread glial cytoplasmic inclusions in the putamen of MSA patient brain (high and low magnification shown, scale bar 100 µm). **(B)** Immunofluorescent analysis with the luminescent conjugated oligothiophene (LCO) h-FTAA shows the absence of aggregates in healthy controls and abundant inclusions in MSA patients. Signal from h-FTAA significantly overlaps with that of pSer129-αSyn (scale bar 40 µm). **(C)** Control MSA mice injected with BSA show pSer129-αSyn

positive cells in the striatum but signal from h-FTAA is largely absent. The absence of h-FTAA in pSer129-αSyn-positive cells indicates that pSer129-αSyn within these cells is either not in an aggregated form or that the aggregates are immature. In contrast, injection of αSyn ribbons or fibrils, results in pSer129-αSyn^{+}/h-FTAA^{+} double positive glial inclusions. Quantification of the two pathological markers shows a similar distribution of **(D)** pSer129-αSyn and **(E)** h-FTAA in MSA human brain (n = 5, mean ± s.e.m., one-tailed unpaired t-test ** P < 0.01). MSA mice injected with different strains showed increased **(F)** pSer129-αSyn and **(G)** h-FTAA positive cells (n = 7-12, mean ± s.e.m., two-way ANOVA with Tukey's multiple comparison test, ** P < 0.01). (**H)** Analysis of pSer129-αSyn^{+}/h-FTAA^{+} double positive cells shows that fibrils and ribbons yield h-FTAA positive aggregates with approximately 25% of pSer129-αSyn^{+} cells whereas in MSA patient brain most cells containing pSer129-αSyn^{+} are also h-FTAA^{+} (n = 7-12, mean ± s.e.m., two-way ANOVA with Tukey's multiple comparison test, ** P < 0.01). Note that in graph (**I**) statistical comparison was performed between experimental groups but not with human samples due to differences in tissue processing and staining methods.

Figure 3. Ribbons and fibrils yield cell-specific inclusions that are structurally distinct. Detection of conformationally distinct assemblies *in vivo* through the use of the conformation sensitive LCO probe h-FTAA. **(A**) To detect aggregate-bearing oligodendendrocytes, neurons, microglia or astrocytes, double labeling with the cell specific markers Olig2, NeuN, Iba-1 or GFAP and h-FTAA was performed (scale bar is 10 µm). **(B)** Confocal image showing GFAP with h-FTAA staining with (**C)** fluorescent intensity of the two emission spectra h-FTAA$_{\lambda 600}$ (magenta) and h-FTAA$_{\lambda 520}$ (green) as a visual representation of the conformational variation in MSA mouse striatum injected with αSyn fibrils (scale bar is 50 µm)**.** Double labeling with GFAP identifies h-FTAA-positive astrocytic inclusions with aggregates also shown in (B) and (C) and are indicated by white arrows. **(D)** Spectral analysis of oligodendroglial inclusions shows the normalized average fluorescent emission spectra obtained from h-FTAA inclusions in MSA control animals, MSA animals injected with ribbons or fibrils and MSA patients brain homogenates. **(E)** The h-FTAA emission spectra between different experimental conditions vary significantly. A wide distribution of h-FTAA$_{\lambda 600/520}$ was detected for the control BSA condition reflecting large heterogeneity of assemblies and the absence of a dominant conformation in this group. Upon seeding with fibrils or ribbons, the relative distribution of h-FTAA$_{\lambda 600/520}$ changes significantly indicative of an altered aggregated state with lower conformational freedom (n = 7, one-way ANOVA with Bonferroni's multiple comparison test, ****P < 0.0001). Note that the spectrum of the oligodendroglial inclusions

triggered by MSA patients brain homogenates is shown as a reference but that statistical comparison with the experimental groups was not performed due to differences in tissue processing. (**F)** Spectra obtained from neuronal inclusions and (**G**) comparison of fluorescent emission spectra in neurons shows that fibrils and ribbons propagate structurally distinct aggregates (**E)** with unique conformational distributions measured via h-FTAA$_{\lambda 600/520}$. **(H)** Spectra obtained from microglial cells **i)** show that different types of aggregates are detected intracellularly (n = 7, unpaired two-tailed t-test, *P < 0.05), **(J**) but not in astrocytes **(K)** where ribbons and fibrils-mediated intracellular inclusions exhibit similar conformational distributions (n = 7, unpaired two-tailed t-test).

Figure 4. Strain-specific microglial activation in MSA mice. (**A**) αSyn ribbons and fibrils trigger significant microglial activation *in vivo.* Activation was measured via Iba1 fluorescent positive area after adaptive triangle thresholding (n = 7-12, mean ± s.e.m., one-way ANOVA with Tukey's multiple comparison test, *** P < 0.001). (**B**) Representative images of Iba1 and CD68 staining in the injected striatum in the three experimental conditions (scale bar is 100 μm). (**C**) The microglial lysosomal marker CD68 is significantly upregulated in MSA mice injected with fibrils and ribbons and is indicative of a differential microglial response between the two strain conditions (n = 7-12, mean ± s.e.m., one-way ANOVA Tukey's multiple comparison test, *** P < 0.001). (**D**) Phagocytic Iba1^{+} microglial cells engulfing pSer129-αSyn inclusions (scale bar is 25 μm). (**E**) The microglial response is accompanied by activation and antigen presentation with MHCII expression. (**F**) Fibrils induce strong MHCII expression in the striatum and corpus callosum.

Figure 5. Characterization of the pro-inflammatory response in primary microglia upon treatment with different αSyn assemblies. (**A**) Immunofluorescent staining for human αSyn (red) and Iba1 (green) of primary microglia treated with different αSyn strains for 24 hours. Scale bar represents 50 μm. Quantification of mRNA levels of (**B**) IL-1β, (**C**) IL6 and (**D**) TNFα, in murine primary microglia upon administration of the two different fibrillar αSyn forms (1 μM). Compared to all other tested conditions, αSyn fibrils trigger a more significant pro-inflammatory phenotype. Untreated cells and cells treated with BSA (1 μM) were included as negative controls. Results shown as mean ± s.e.m., with three unique cell culture experiments at different time points with different assemblies (*P < 0.05, for one-way ANOVA with Tukey's post-hoc analysis; n = 3).

Figure 6. Astrocytic activation and intracellular inclusion formation by αSyn strains. (**A**) Striatal injection of ribbons and fibrils in MSA mice cause significant activation of astrocytes (n = 7-12, mean ± s.e.m., two-way ANOVA Tukey's Multiple Comparison test, ***P < 0.001). (**B**)

Ribbons induce significantly more pSer129-αSyn inclusions in astrocytes compared to the fibrils condition (n = 7-12, mean ± s.e.m., two-way ANOVA Tukey's Multiple Comparison test, ***P < 0.001). (**C**) Representative images of GFAP expression of the different experimental and control conditions. (**D**) Colocalization of pSer129-αSyn and GFAP shows intracellular glial accumulation of αSyn (scale bar is 25 μm).

Figure 7. Widespread infiltration of peripheral immune cells in MSA mice after αSyn fibrils injection. (**A**) The specific microglial marker Tmem119 allows distinguishing brain from peripheral macrophages. Co-labeling with Iba1 shows that in the control MSA mice, Tmem119 exclusively colocalizes with Iba-1 (n = 7-12, mean ± s.e.m., one-way ANOVA with Tukey's multiple comparison test, ***P < 0.001). In animals injected with fibrils and ribbons, Tmem119 expression is absent in a subpopulation of Iba-1 cells, suggesting that these macrophages are non-resident immune cells. (**B**) Representative images of Iba1 and Tmem119 in the different conditions showing resident (Tmem119$^+$) and peripheral macrophages (Tmem119$^-$, white arrows) (scale bar = 50μm). (**C**) Peripheral immune cells, detected via the marker CD45, which is highly expressed in all hematopoietic cells, are detected throughout the brain in the fibril condition but are absent in other conditions (n = 7-12, mean ± s.e.m., one-way ANOVA with Tukey's multiple comparison test, **P < 0.01, ***P < 0.001). (**D**) CD45$^+$ cells infiltrate the brain via blood vessels in the corpus callosum and the striatum. Arrows in the middle panel indicate blood vessels and CD45$^+$ cells aligned along the vessels. The right panel shows a higher magnification of infiltrating peripheral immune cells. (**E**) Quantification of CD3$^+$ T cells (n = 7-12, Mean ± SEM, one-way ANOVA Tukey's multiple comparison test, *P < 0.05, ****P < 0.0001) and f) representative images for infiltrating T cells.

Table 1 Brain tissue from controls and multiple system atrophy cases used in this study

Case	Gender	Age	Region
Control	Male	70	Putamen
Control	Male	50	Putamen
Control	Male	61	Putamen
Control	Female	60	Putamen
Control	Female	69	Putamen
MSA-P	Female	60	Putamen
MSA-P	Female	74	Putamen
MSA-P	Male	63	Putamen
MSA-P	Male	65	Putamen
MSA-P	Male	51	Putamen

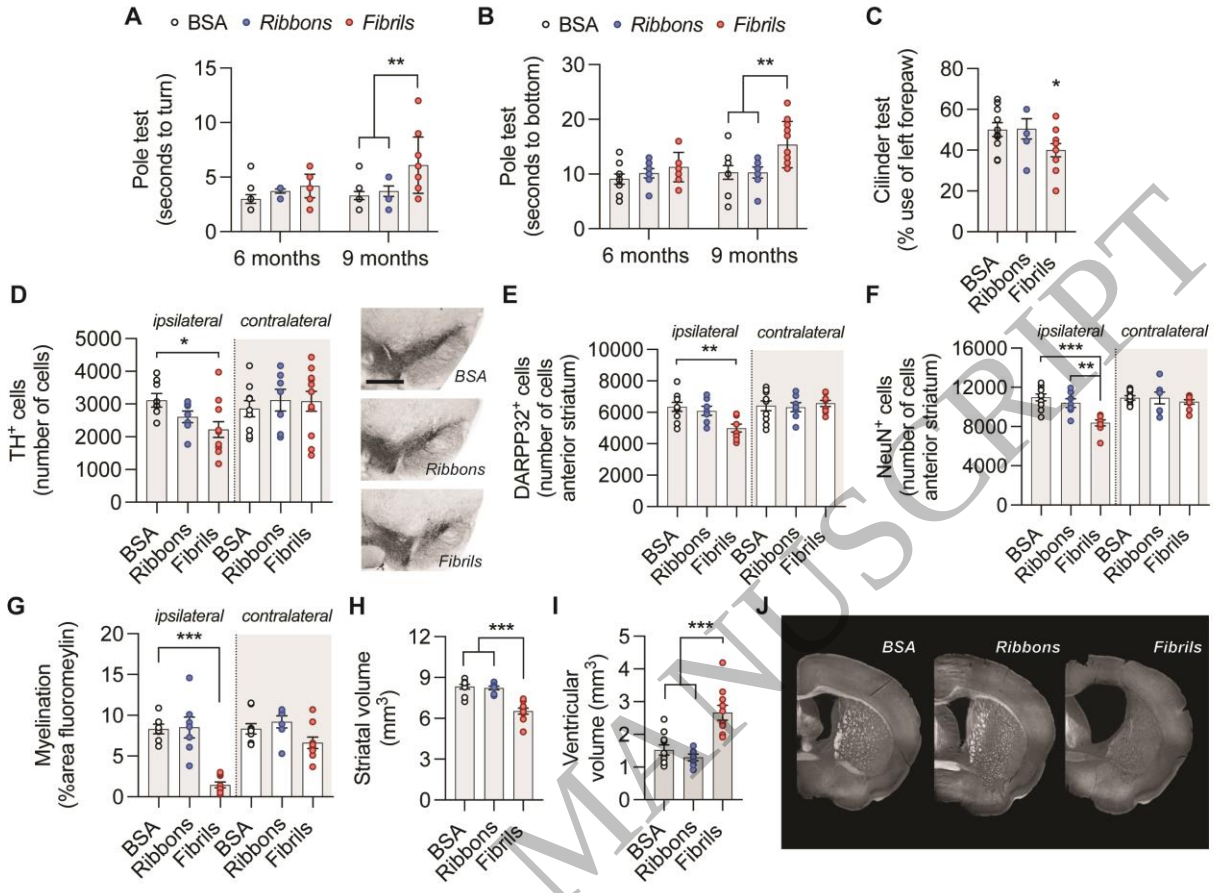

Figure 1
216x156 mm (4.7 x DPI)

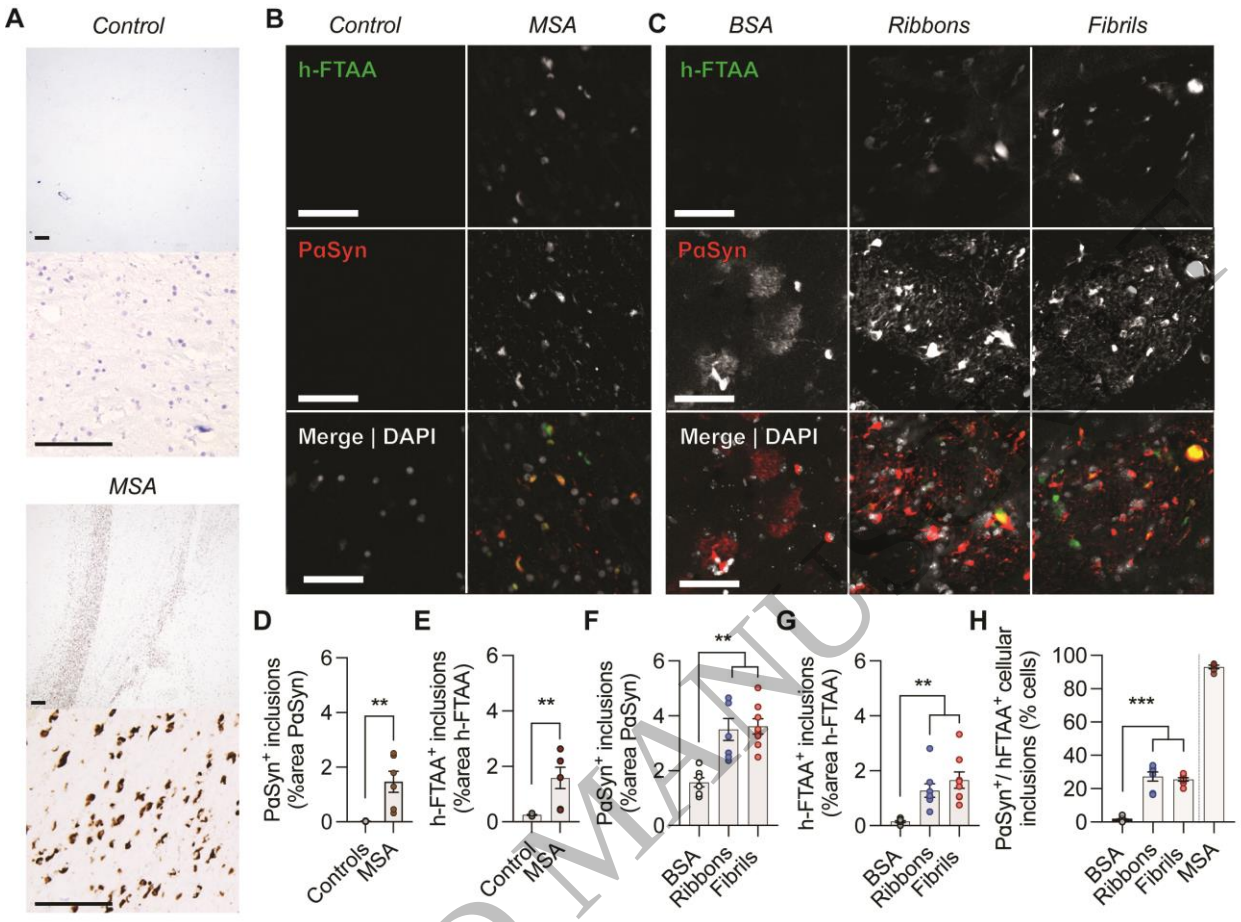

Figure 2
196x145 mm (4.7 x DPI)

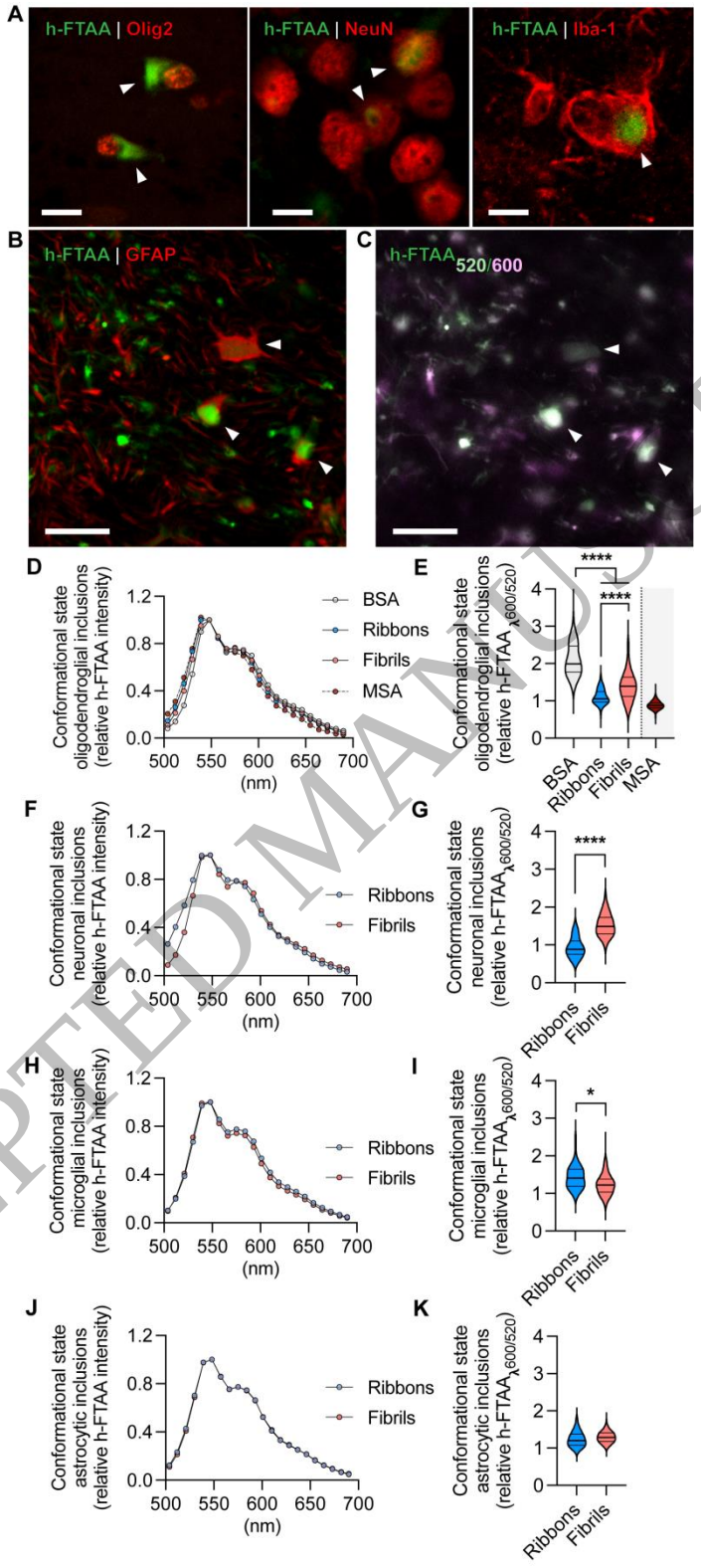

Figure 3
129x297 mm (4.7 x DPI)

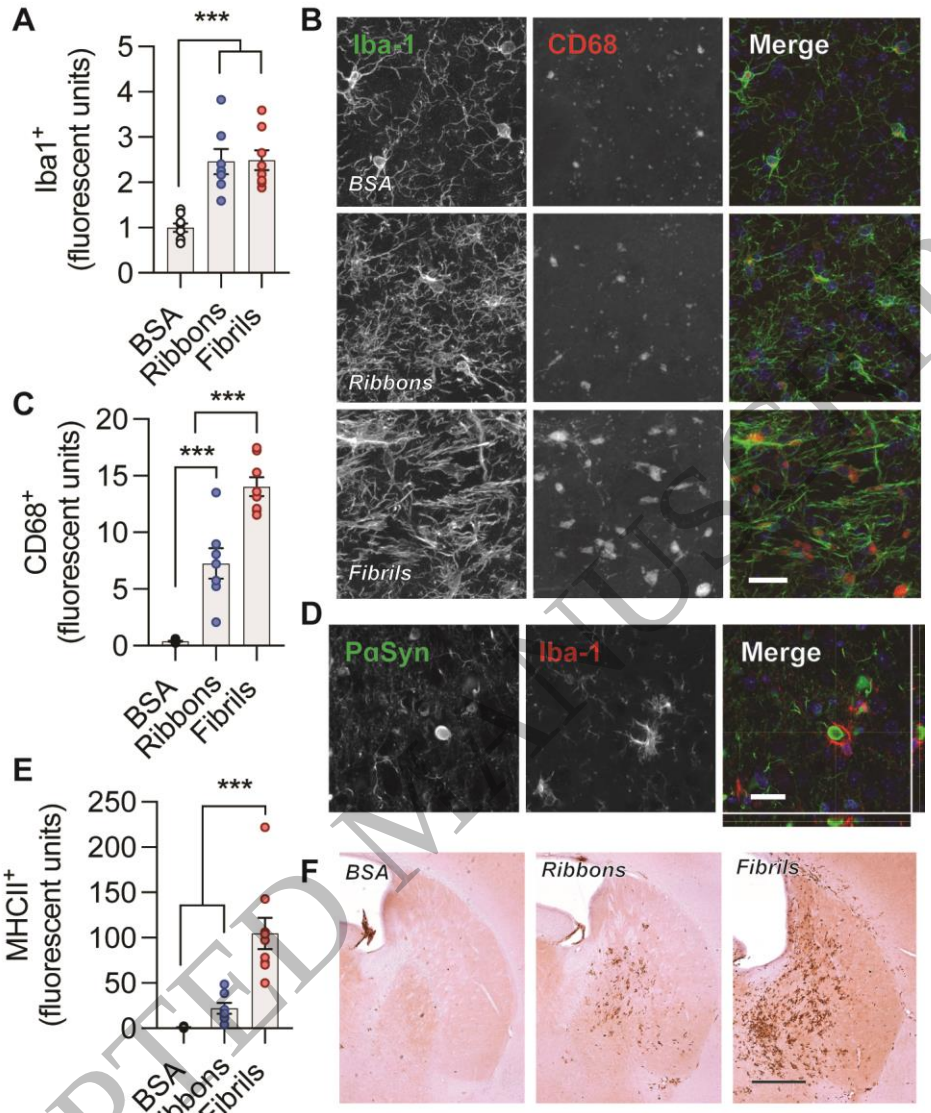

Figure 4
126x157 mm (4.7 x DPI)

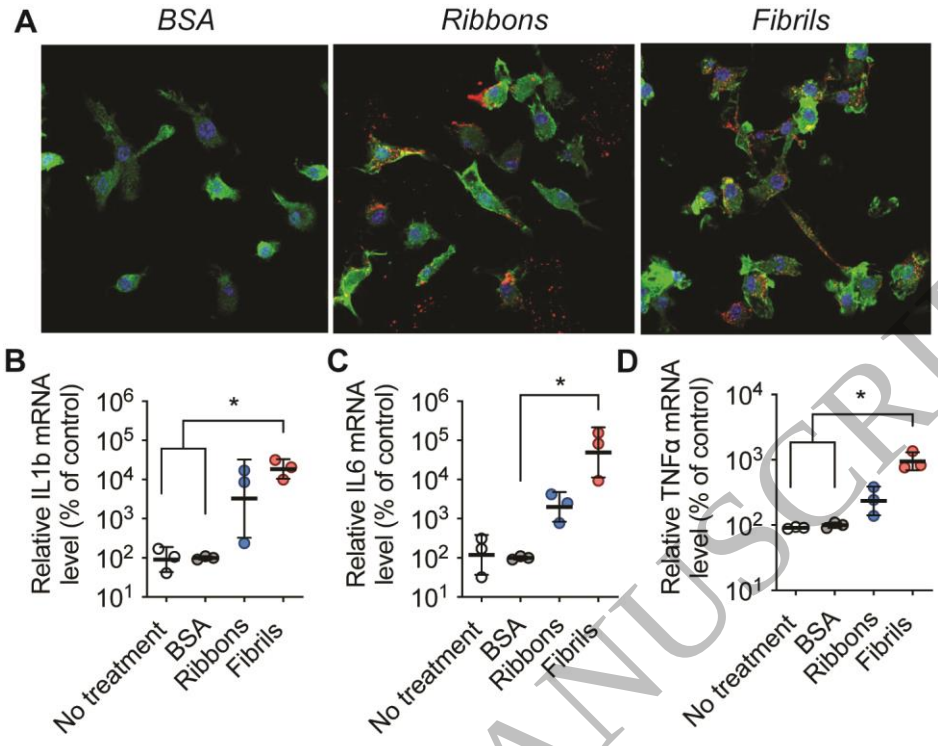

Figure 5
127x100 mm (4.7 x DPI)

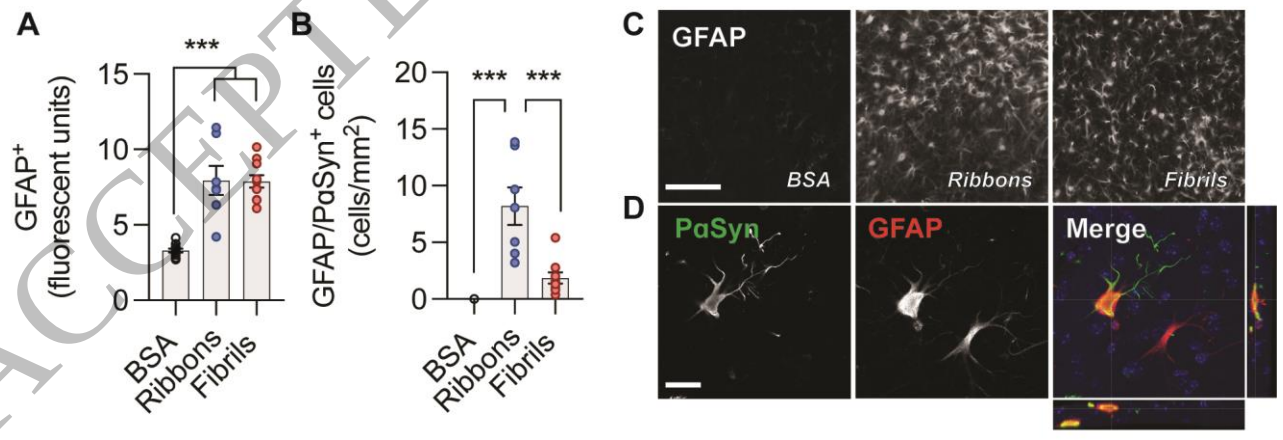

Figure 6
172x57 mm (4.7 x DPI)

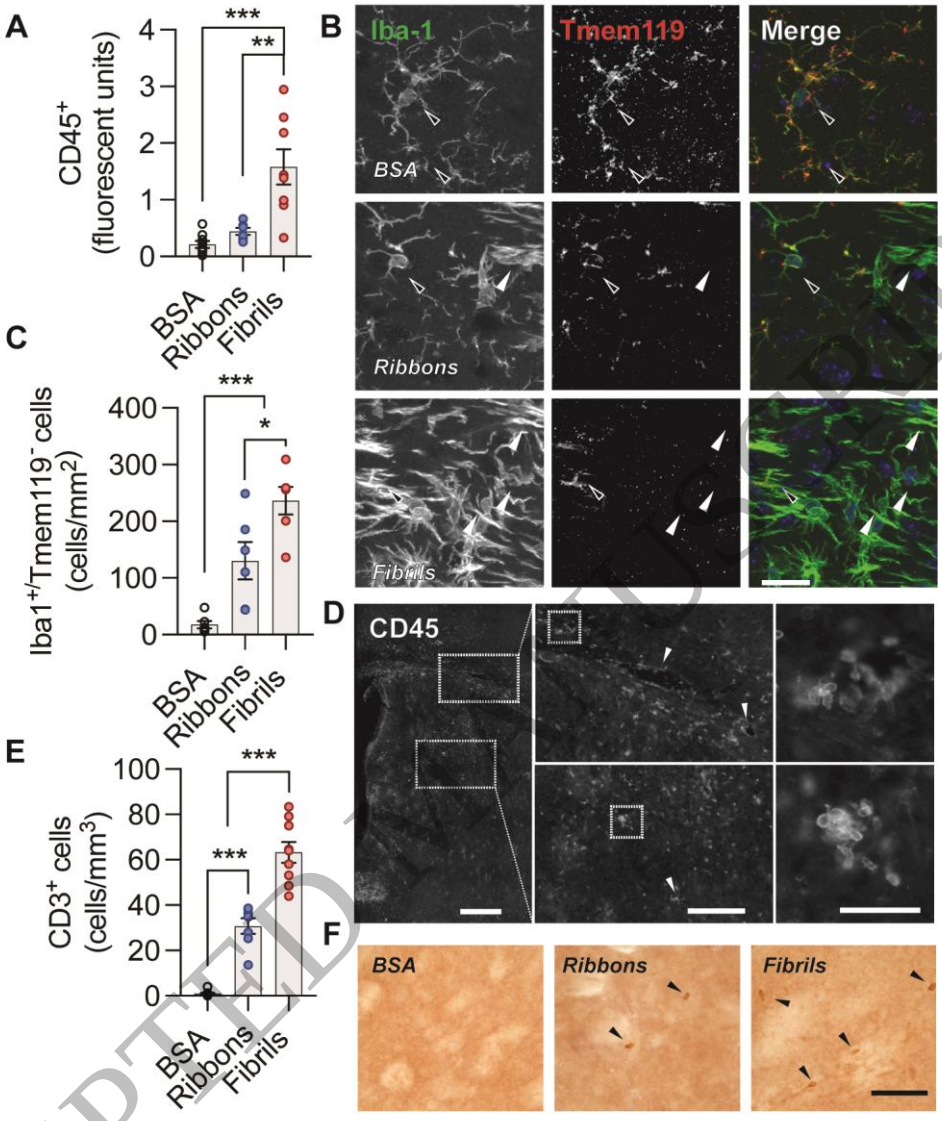

Figure 7
126x153 mm (4.7 x DPI)